Evidence for πK-atoms with DIRAC

B. Adeva [o], L. Afanasyev [l], Y. Allkofer [r,*], C. Amsler [r,*], A. Anania [f], A. Benelli [r], V. Brekhovskikh [n], G. Caragheorgheopol [k], T. Cechak [b], M. Chiba [j], P. Chliapnikov [n], C. Ciocarlan [k], S. Constantinescu [k], C. Curceanu [e], C. Detraz [a], D. Dreossi [g], D. Drijard [a], A. Dudarev [l], M. Duma [k], D. Dumitriu [k], J.L. Fungueiriño [o], J. Gerndt [b], A. Gorin [n], O. Gorchakov [l], K. Gritsay [l], C. Guaraldo [e], M. Gugiu [k], M. Hansroul [a], Z. Hons [d], S. Horikawa [r], M. Iliescu [e], V. Karpukhin [l], J. Kluson [b], M. Kobayashi [h], V. Komarov [l], V. Kruglov [l], L. Kruglova [l], A. Kulikov [l], A. Kuptsov [l], I. Kurochkin [n], A. Lamberto [f], A. Lanaro [e], V. Lapshin [n], R. Lednicky [c], P. Levi Sandri [e], A. Lopez Aguera [o], V. Lucherini [e], I. Manuilov [n], C. Mariñas [o], L. Nemenov [l], M. Nikitin [l], K. Okada [i], V. Olchevskii [l], M. Pentia [k], A. Penzo [g], M. Pló [o], G.F. Rappazzo [f], C. Regenfus [r], J. Rochet [r], A. Romero [o], V. Ronjin [n], A. Ryazantsev [n], V. Rykalin [n], J. Saborido [o], J. Schacher [q], A. Sidorov [n], J. Smolik [c], S. Sugimoto [h], F. Takeutchi [i], A. Tarasov [l], L. Tauscher [p,1], T. Trojek [b], S. Trusov [m], V. Utkin [l], O. Vázquez Doce [e,o], T. Vrba [b], V. Yazkov [m], Y. Yoshimura [h], M. Zhabitsky [l], P. Zrelov [l]

[a] *CERN, Geneva, Switzerland*
[b] *Czech Technical University, Prague, Czech Republic*
[c] *Institute of Physics ACSR, Prague, Czech Republic*
[d] *Nuclear Physics Institute ASCR, Rez, Czech Republic*
[e] *INFN, Laboratori Nazionali di Frascati, Frascati, Italy*
[f] *INFN, Messina University, Messina, Italy*
[g] *INFN, Trieste University, Trieste, Italy*
[h] *KEK, Tsukuba, Japan*
[i] *Kyoto Sangyo University, Kyoto, Japan*
[j] *Tokyo Metropolitan University, Japan*
[k] *IFIN-HH, National Institute for Physics and Nuclear Engineering, Bucharest, Romania*
[l] *JINR Dubna, Russia*
[m] *Skobeltsin Institute for Nuclear Physics of Moscow State University, Moscow, Russia*
[n] *IHEP Protvino, Russia*
[o] *IGFAE, Santiago de Compostela University, Spain*
[p] *Basel University, Switzerland*
[q] *Bern University, Switzerland*
[r] *Physik-Institut der Universität Zürich, Switzerland*

ARTICLE INFO

ABSTRACT

We present evidence for the first observation of electromagnetically bound $\pi^\pm K^\mp$-pairs (πK-atoms) with the DIRAC experiment at the CERN-PS. The πK-atoms are produced by the 24 GeV/c proton beam in a thin Pt-target and the $\pi^\pm$ and $K^\mp$-mesons from the atom dissociation are analyzed in a two-arm magnetic spectrometer. The observed enhancement at low relative momentum corresponds to the production of 173 ± 54 πK-atoms. The mean life of πK-atoms is related to the s-wave πK-scattering lengths, the measurement of which is the goal of the experiment. From these first data we derive a lower limit for the mean life of 0.8 fs at 90% confidence level.

* Corresponding authors.
 E-mail address: claude.amsler@cern.ch (C. Amsler).
[1] This publication is dedicated to the memory of Ludwig Tauscher.

1. Introduction

The study of electromagnetically bound hadronic pairs is an excellent method to probe QCD at very low energy. Opposite charge long-lived hadrons such as pions and kaons can form hydrogen-like atoms bound by the Coulomb interaction. The strong interaction leads to a broadening of the atomic levels and dominates the lifetime of the atom.

Pion–pion interaction at low energy, constrained by the approximate 2-flavour SU(2) (u, d) chiral symmetry, is the simplest and well understood hadron–hadron process [1–3]. The observation of $\pi^+\pi^-$-atoms $(A_{2\pi})$ was reported in Ref. [4] and a measurement of their mean life in Ref. [5].

The low energy interaction between the pion and the heavier (strange) kaon is a tool to study the more general 3-flavour SU(3) (u, d, s) structure of hadronic interaction, which is not accessible in $\pi\pi$-interactions. A detailed study of πK-interaction provides insights into a potential flavour (u, d, s) dependence of the crucial order parameter or quark condensate in Chiral Perturbation Theory (ChPT) [6].

A measurement of the πK-atom $(A_{\pi K})$ lifetime was proposed already in 1969 [7] to determine the difference $|a_{1/2} - a_{3/2}|$ of the s-wave πK-scattering lengths, where the indices 1/2 and 3/2 refer to the isospin of the πK-system. The $\pi^\pm K^\mp$-atom decays predominantly by strong interaction into the neutral meson pair $\pi^0 K^0$ $(\pi^0 \overline{K}^0)$. The decay width of the πK-atom in the ground state is given by the relation [7,8]:

$$\Gamma(A_{\pi K}) = \frac{1}{\tau_{1S}} = \frac{8}{9}\alpha^3\mu^2 p^* |a_{1/2} - a_{3/2}|^2 (1 + \delta). \tag{1}$$

τ_{1S} is the lifetime of the atom in the ground state, α the fine structure constant, μ the reduced $\pi^\pm K^\mp$ mass, and $p^* = 11.8$ MeV/c the outgoing K^0 or π^0 3-momentum in the πK center-of-mass system. The term $\delta \simeq (4 \pm 2)\%$ [8] accounts for corrections, due to isospin breaking and the quark mass difference $m_u - m_d$. Hence a measurement of $\Gamma(A_{\pi K})$ provides a value for the scattering length $|a_{1/2} - a_{3/2}|$. The mean life of πK-atoms is predicted to be 3.7 ± 0.4 fs [8].

The width $\Gamma(A_{\pi K})$ can also be determined from the s-wave phase shifts obtained from πK-scattering, i.e. from the interaction of kaons with nucleons. The s-wave phase shifts are, however, poorly known due to the absence of data below 600 MeV/c and, correspondingly, the uncertainties in $a_{1/2}$ and $a_{3/2}$ are substantial. The overall interaction is attractive (attractive in the isospin 1/2 and repulsive in the 3/2 state). The Roy–Steiner equations lead, with the available scattering data, to results [9] that are neither consistent with the most precise measurements [10] nor with predictions from ChPT [11].

The method used by DIRAC is to produce pions and kaons with a high energy proton beam impinging on a thin target. Pairs of oppositely charged mesons may interact and form electromagnetically bound systems. Their subsequent ionization in the production target leads to mesons emerging from the target with low relative momentum (thereafter called atomic pairs). The mean life of the πK-atom can then be calculated from the number of observed low-momentum pairs. This method was first proposed in 1985 [12] and was successfully applied to $\pi^+\pi^-$-atoms in Serpukhov on the U-70 synchrotron internal proton beam [4], and with DIRAC-I at the CERN-PS on beam line T8. Data from DIRAC-I lead to a mean life $\tau_{2\pi} = (2.91^{+0.49}_{-0.62})$ fs for $\pi^+\pi^-$-atoms [5].

Cross sections for $A_{\pi K}$-production have been calculated in Ref. [13]. In this Letter we report on the observation of πK-atoms from the first data with DIRAC-II.

2. Experimental setup

Details on the initial apparatus (DIRAC-I) used to study $\pi^+\pi^-$-atoms can be found in Ref. [14]. A sketch of the modified spectrometer (DIRAC-II) used to collect the πK (and more $\pi\pi$) data is shown in Fig. 1. The 24 GeV/c proton beam (1) from the CERN-PS impinges on a 26 μm Pt-target (2). The spill duration is 450 ms with an average intensity of 1.6×10^{11} protons/spill. The proton beam then passes through a vacuum pipe and is absorbed by the beam dump. The secondary particles are collimated through two steel shielding blocks (3) and (7), upstream of the microdrift chambers (4) and downstream of the ionization hodoscope (6), respectively. They pass through a vacuum chamber (8) and are bent by the 1.65 T field of the dipole magnet (9). The two-arm spectrometer is tilted upwards with respect to the proton beam by an angle of 5.7°. Positive particles are deflected into the left arm, negative ones into the right arm.

We now describe in more detail the upgrade which was performed to search for and study πK-atoms [15]. The upstream detectors (4–6), see Fig. 1, were either replaced or upgraded. However, they were not yet fully operational during data taking, and were therefore not used in the analysis presented here. The tracking is performed by drift chambers (10) which have a spatial resolution of 85 μm. The vertical hodoscope (11) consisting of 20 scintillating slabs with a time resolution below 140 ps is used for timing. The horizontal hodoscope (12), made of 16 horizontal scintillating slabs, is used for triggering by selecting oppositely charged particles with a vertical displacement smaller than 75 mm.

The N$_2$-Čerenkov detector (15) was already used previously to reject electrons and positrons. The refractive index is $n = 1.00029$ and the average number of photoelectrons $N_{pe} = 16$ for particles with velocity $\beta = 1$. The inner part of the original container had to be cut to clear space for the two new Čerenkov detectors needed for kaon identification. Since the momenta of the two mesons originating from the breakup of the πK-atoms are very small in the center-of-mass system, they have similar velocities in the laboratory system, and hence kaons are less deflected than pions. Typical trajectories are shown in Fig. 1.

The heavy gas C$_4$F$_{10}$-Čerenkov detectors in both arms (14) identify pions but do not respond to kaons nor (anti)protons [16]. Four spherical and four flat mirrors each focus the light towards the phototubes. The alignment of the mirrors was checked with a laser beam [17]. To keep a constant refractive index of $n = 1.0014$, the gas has to be cleaned permanently with a complex recirculating system [18]. The average number of photoelectrons is 28 for particles with $\beta = 1$.

The aerogel Čerenkov detector (13) in the left arm identifies kaons and rejects protons [19,20]. Such a detector is required only in the left arm since the contamination from antiprotons in the right arm is small due to their low production rate. The detector consists of three modules. Two modules of 12ℓ each (refractive index $n = 1.015$) cover the relevant momentum range between 4 and 8 GeV/c. The aerogel stacks are 42 cm high and are read out by two 5″-Photonis XP4570 photomutipliers with UV windows. The typical number of photoelectrons is 10 for $\beta = 1$ particles. A third overlapping module with 13ℓ aerogel and $n = 1.008$ cov-
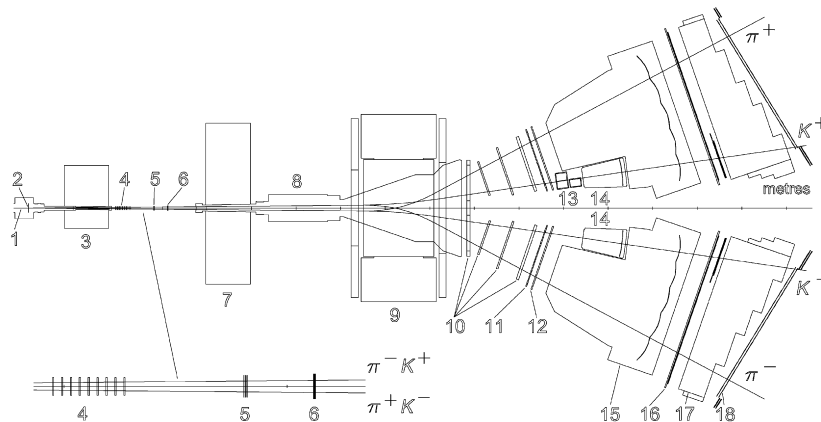
Fig. 1. Sketch of the DIRAC-II spectrometer (top view). 1 – proton beam, 2 – production target, 3 – shielding, 4 – microdrift chambers, 5 – scintillation fiber detector, 6 – ionization hodoscope, 7 – shielding, 8 – vacuum chamber, 9 – dipole magnet, 10 – drift chambers, 11 – vertical hodoscope, 12 – horizontal hodoscope, 13 – aerogel Čerenkov modules, 14 – heavy gas Čerenkov detector, 15 – N$_2$-Čerenkov detector, 16 – preshower detector, 17 – absorber, 18 – muon scintillation hodoscope. The solid lines crossing the spectrometer arms correspond to typical $\pi^{\pm}$- and $K^{\mp}$-trajectories from the ionization of πK-atoms in the production target.

ers the small angle region to reject protons with momenta above 5.3 GeV/c.

The aerogel tiles are stacked pyramidally to increase the radiator thickness halfway between the photomutipliers and to compensate for light absorption. Due to the low light yield for the $n = 1.008$ module, and the strong UV-light absorption, we use a wavelength shifter. The aerogel tiles are sandwiched between Tetratex foils on which tetraphenylbutadiene (TPB) has been evaporated [19]. The typical number of photoelectrons is 4–8 for $\beta = 1$ particles.

The preshower detector **(16)** provides additional electron/hadron separation in the offline analysis. A lead converter, typically 10–25 mm thick, is placed in front of a 10 mm thick scintillator. An additional converter/scintillator is installed to compensate for the drop of efficiency of the N$_2$-Čerenkov detector at small angles, in the region covered by the aerogel and heavy gas detectors. The iron absorber **(17)** and the array of scintillation counters **(18)** are used to suppress muons.

Pairs such as e^+e^-, $\pi^+\pi^-$, π^-K^+ or π^+K^- are selected by a two-level trigger. For π^-K^+- and π^+K^--candidates the first level trigger requires no signal in the heavy gas detector of the K-arm and in the N$_2$-Čerenkov detectors. The two tracks have to cross the same (or one of the two adjacent) slab(s) in each of the horizontal hodoscopes. The two trajectories being asymmetric (see Fig. 1), the kaon is required to cross slabs of the vertical hodoscope located in front of the heavy gas detector, while the associated pion has to fly at large angles in the opposite arm. The second level trigger [21] uses raw hits from the drift chambers and, based on a lookup table, rejects pairs with high relative momentum. The accepted trigger rate is limited by the buffer memory of around 2000 events per spill.

3. Tracking and calibration

As mentioned already, only detectors downstream of the dipole magnet are used here for event reconstruction. The trajectories are determined by the drift chambers, the pattern recognition starting from the horizontal x-coordinate in the last plane and extrapolating back to the target. A straight line is first fitted through the hits and extended into the magnet yoke. A deflection algorithm [22] calculates the slope and x-coordinate of the track at the magnet entrance, following the magnetic field map. The trajectory is then extrapolated linearly to the target, with the constraint that the track origin has to coincide with the center of the beam spot. This determines the momentum of the particle. For the vertical y-coordinate the straight line from the drift chamber information is
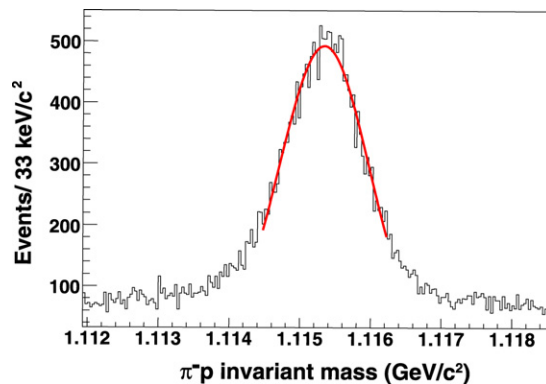

Fig. 2. π^-p-mass distribution in the Λ-region. The line shows the Gaussian fit.
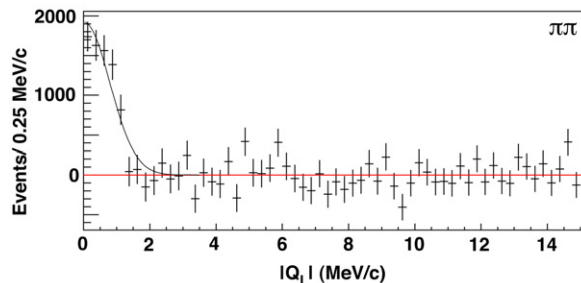

Fig. 3. Q_L-distribution measured with DIRAC-II for part of the $\pi^+\pi^-$ data after background subtraction. The accumulation of events at low Q_L is due to $\pi^+\pi^-$-atoms. The curve is a Gaussian fit to guide the eye.

extrapolated back to the center of the beam spot at the production target [23,24].

The variable of interest in the following analysis is the relative momentum Q of the $K^{\pm}\pi^{\mp}$-pairs in their center-of-mass systems. In the transverse plane, the resolution on the relative momentum Q_T (typically 3 MeV/c) is dominated by multiple scattering, while the resolution on the longitudinal component Q_L (<1 MeV/c) is not affected [23,25]. For further analysis we use therefore only Q_L.

The momentum calibration was cross-checked with tracks from $\Lambda \to \pi^- p$ decays. Fig. 2 shows the invariant π^-p-mass distribution. A Gaussian fit is applied leading to a mass of 1115.35 $\pm$ 0.08 MeV/c^2 (statistical error) and a width of $\sigma = 0.58 \pm 0.01$ MeV/c^2, dominated by momentum resolution.

We have verified that the new hardware and software were able to reproduce the signal from $\pi^+\pi^-$-atoms. Details of the procedure for $\pi^+\pi^-$ atoms can be found in Refs. [5,23]. Fig. 3 shows
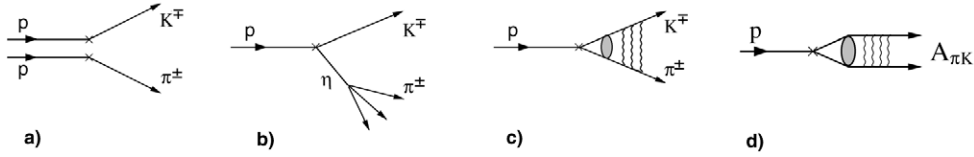
Fig. 4. Production mechanisms of πK-pairs: (a) accidental-pairs from two protons; (b) non-Coulomb-pairs from long-lived intermediate states such as the η-meson; (c) Coulomb-pairs from direct production or from short-lived intermediate states; (d) πK-atoms.

the momentum distribution after background subtraction. The enhancement at low Q_L corresponds to 7098 ± 533 atomic $\pi^+\pi^-$-pairs. Bound $\pi^+\pi^-$-pairs are not expected above $|Q_L| = 2$ MeV/c and indeed the distribution in Fig. 3 is flat and compatible with zero, which validates the background subtraction method. Note that the present data cannot be compared directly with those of Ref. [5] because we used here only the downstream detectors, and a different event selection was performed.

4. Data analysis

Fig. 4 shows the four mechanisms which contribute to the production of $\pi^\pm K^\mp$-pairs. Accidental pairs are due to particles produced on different nucleons (Fig. 4(a)), non-Coulomb-pairs are associated with the production of long-lived intermediate states (Fig. 4(b)). On the other hand, $\pi^\pm K^\mp$-pairs which interact electromagnetically form correlated Coulomb-pairs (Fig. 4(c)), or atomic bound states (Fig. 4(d)). The N^A atoms, while traveling through the target, can either decay, be (de-)excited or break up into n^A $\pi^\pm K^\mp$-pairs which emerge from the target with very low relative momentum.

We now describe the analysis steps [23]. For prompt pairs the time difference between the positive and negative spectrometer arm lies between -0.5 and 0.5 ns. Accidental pairs are first removed using the time information from the vertical hodoscopes. Accidental pairs are also needed for subsequent analysis and we select those pairs with a time difference between -12 and -6 ns. The choice of the negative sign avoids the contamination from slow protons. The events have then to satisfy the following criteria:

- no electrons nor positrons,
- no muons,
- one drift chamber track per arm,
- $|Q_L| < 20$ MeV/c,
- $Q_T < 8$ MeV/c,
- the momentum of the kaon lies between 4 GeV/c and 8 GeV/c,
- the momentum of the pion lies between 1.2 GeV/c and 2.1 GeV/c.

With the excellent time resolution of the vertical hodoscope pions, kaons and protons below 2.5 GeV/c can be separated by time-of-flight [26]. For the π^-K^+ analysis the aerogel detector is used in addition to remove protons in the positive arm, while for the π^+K^- analysis, the time difference between the negative and the positive arm measured with the vertical hodoscope has to be negative in order to remove protons faking pions. Once the accidentals have been subtracted the prompt pairs (N^{pr}) are composed of the following three types: atomic-pairs (n^A), Coulomb-pairs (N^C), and non-Coulomb-pairs (N^{nC}). Therefore

$$N^{pr} = n^A + N^C + N^{nC}. \tag{2}$$

However, the background arising from $\pi^+\pi^-$- and π^-p-pairs with misidentified particles must be considered since the kaon flux is much lower than the pion and proton fluxes. Pions can

be selected with the heavy gas detector in coincidence and protons with the aerogel detector in anticoincidence. We then determine Q_L by assigning to the pion (or the proton) the mass of a kaon. For $\pi^+\pi^-$ events this incorrect mass assignment shifts the Q_L-distribution by -150 MeV/c [23] and therefore does not overlap with the Q_L-distribution of πK events. The contribution from π^-p-pairs, non-Coulomb π^-K^+-pairs and accidentals have a similar linear Q_L-distribution. We assume that the background due to Coulomb uncorrelated pairs can be described by the Q_L-distribution of accidentals, following a similar analysis for $\pi^+\pi^-$-atoms [5]. The non-Coulomb background also includes the background from π^-p-pairs. Coulomb correlated pairs have to be simulated [27,28].

To determine the contribution from Coulomb- and non-Coulomb pairs we select the momentum range $3 < |Q_L| < 20$ MeV/c, where no atoms are expected. The Q_L-distribution is

$$\frac{dN^{pr}}{dQ_L} = \beta \cdot \frac{dN^C}{dQ_L} + \left(N^{pr} - \beta\right) \cdot \frac{dN^{acc}}{dQ_L}, \tag{3}$$

where dN^C/dQ_L and dN^{acc}/dQ_L are the (normalized) differential probabilities for Coulomb correlated or uncorrelated pairs, respectively. The fit variable β is the corresponding number of correlated pairs. We choose a bin size of 0.25 MeV/c. The χ^2-function to be minimized is

$$\chi^2 = \sum_{|i|=13}^{80} \left[\frac{\frac{dN^{pr}}{dQ_{L,i}} - \beta \cdot \frac{dN^C}{dQ_{L,i}} - (N^{pr} - \beta) \cdot \frac{dN^{acc}}{dQ_{L,i}}}{\sigma_i^{pr}} \right]^2, \tag{4}$$

where σ_i^{pr} are the corresponding statistical errors in the measured number of prompt pairs. Fig. 5(a) shows the MINUIT results for Coulomb- and non-Coulomb contributions to π^-K^+ events. Since the shapes of both contributions are known, one can extrapolate into the $|Q_L| < 3$ MeV/c signal region. The difference (residuals) between the data and the sum of both contributions is plotted in Fig. 5(b). Above $|Q_L| = 3$ MeV/c the residuals are consistent with zero, while the enhancement at low relative momentum is the first evidence for π^-K^+-atoms.

A Gaussian distribution describes adequately the low momentum enhancement observed in the $\pi^+\pi^-$ data [23]. To guide the eye we also apply a Gaussian fit here (line in Fig. 5(b)). The integral of the Gaussian distribution contains 147 ± 61 atomic π^-K^+-pairs.

A similar fit based on Eq. (4) is applied to π^+K^- events. However, the number of events is smaller, due to the lower production cross section for negative kaons. The fit results are summarized in Table 1. The errors on the number of Coulomb-pairs β are the full (MINOS) errors, while the errors on n^A are given by the square roots of the measured bin contents, statistical fluctuations on the much larger Monte Carlo sample being negligible.

Fig. 6 shows the sum of the π^-K^+ and π^+K^- residuals. We obtain

$$n^A(\pi^\pm K^\mp) = 173 \pm 54 \tag{5}$$

detected atomic pairs with a statistical significance of 3.2σ. The systematic uncertainty is estimated to be around 5%, much smaller than the statistical one.
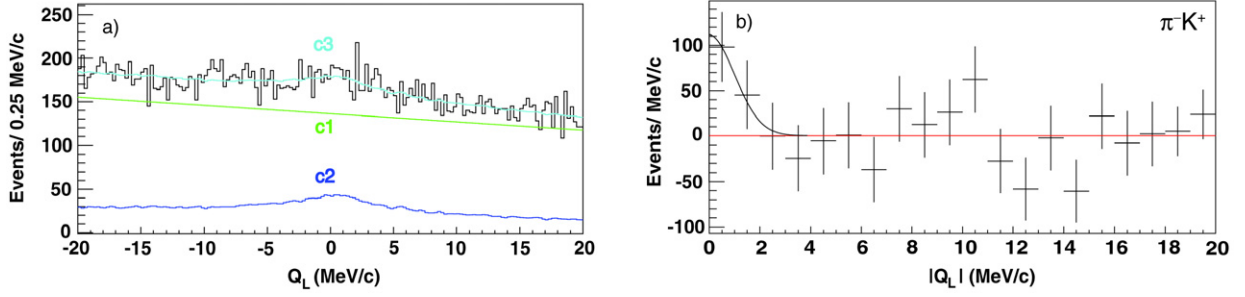
Fig. 5. (a) Q_L-distributions for the $\pi^- K^+$ data sample (26 μm Pt-target). The histogram shows the data. The fitted non-Coulomb- and Coulomb-pairs are in green (c1) and blue (c2) respectively, together with the total background in turquoise (c3). (b) Residuals between data and fitted background. The solid line illustrates the distribution of atomic-pairs (see text). (For interpretation of the references to colour in this figure legend, the reader is referred to the web version of this Letter.)
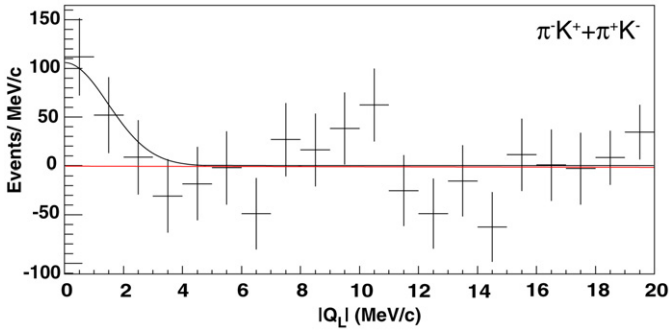

Fig. 6. Residuals between data and the fitted background for $\pi^- K^+$ and $\pi^+ K^-$. A Gaussian fit has been applied (solid line) to illustrate the distribution of atomic-pairs.
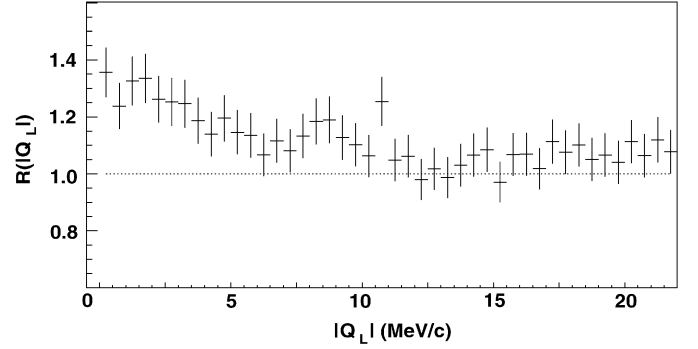

Fig. 7. Correlation function R as a function of $|Q_L|$ for $\pi^- K^+$-pairs. The deviation from the horizontal dotted line proves the existence of Coulomb correlated $\pi^- K^+$-pairs.

Table 1
Left: number β of Coulomb-pairs outside the signal region ($3 < |Q_L| < 20$ MeV/c), number N^C of Coulomb-pairs extrapolated into the signal region ($|Q_L| < 3$ MeV/c), and number n^A of detected atomic-pairs from the residuals of the fit. Right: expected number of atoms N_e^A, calculated from the number of detected Coulomb-pairs, and expected number of atomic pairs n_e^A using a breakup probability of 53%.

χ^2-minimization					Expected	
Atom	χ^2/ndof	β	N^C	n^A	N_e^A	n_e^A
$\pi^- K^+$	0.92	4215	972	143	204	108
		±1008	±233	±53	±59	±31
$\pi^+ K^-$	1.24	1356	164	29	74	39
		±396	±108	±15	±35	±19

The evidence for the observation of πK-atoms is strengthened by the observation of correlated Coulomb-pairs which, a fortiori, implies that atoms have also been produced. This can be seen as follows, without involving simulation: non-Coulomb pairs have a similar Q_L-distribution as accidentals. Hence dividing the normalized distribution for prompt pairs by the one for accidentals one obtains the correlation function R describing Coulomb-pairs. The function R, shown in Fig. 7 for $\pi^- K^+$ as a function of $|Q_L|$, is clearly increasing with decreasing momentum, proving that Coulomb-pairs have been observed. In the signal region ($|Q_L| < 3$ MeV/c) one obtains 858 ± 247 Coulomb-pairs from the data in Fig. 7, without resorting to Monte Carlo. The same procedure can be applied to $\pi^+ K^-$ events, leading to 313 ± 148 Coulomb-pairs [23].

The ratio k of the number of produced atoms to the number of Coulomb-pairs with small relative momenta has been calculated: $k = 0.62$ [12,29]. However, one needs to take into account the acceptance of the apparatus and the cuts applied in the analysis. By Monte Carlo simulation [30] we determine the ratio $k_{\exp} = 0.24$ between the number of atoms produced within acceptance and the number of detected Coulomb-pairs below $|Q_L| = 3$ MeV/c (and below $Q_T = 8$ MeV/c). This then leads to the expected number N_e^A
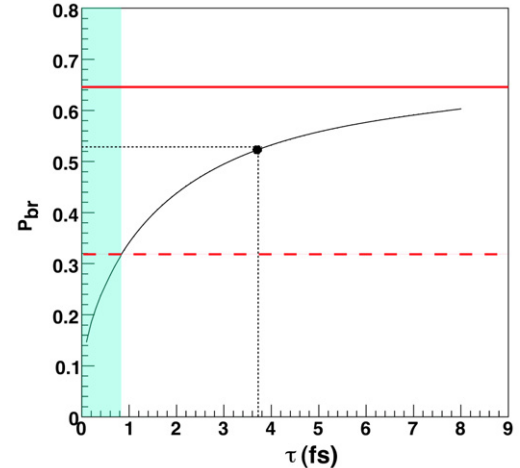

Fig. 8. Breakup probability P_{br} for the 26 μm Pt-target as a function of mean life of πK-atoms in the $1S$-state. The horizontal solid line is the measured breakup probability and the horizontal dashed line the 1.28σ lower bound corresponding to a lower limit of 0.8 fs for the mean life. The excluded area (90% confidence level) is shown in turquoise. The horizontal dotted line gives the theoretical prediction [8].

of atoms, 204 ± 59 for $\pi^+ K^-$, and 74 ± 35 for $\pi^- K^+$ (Table 1, right). The uncertainty on $k_{\exp}$ is negligible.

The breakup probability

$$P_{br} = \frac{n_e^A}{N_e^A} \tag{6}$$

relates the number of atoms to the number of atomic pairs. A calculation of the breakup probability as a function of mean life (Fig. 8) has been performed using the Born approximation [15]. For the predicted mean life of 3.7 ± 0.4 fs [8] the corresponding

breakup probability P_{br} is 53% (dotted line in Fig. 8). From Eq. (6) we then find the number n_e^A of expected pairs given in Table 1, right. These numbers are in good agreement with the number n^A of observed atomic-pairs (fifth column in Table 1).

Conversely, we use the number of observed atomic-pairs n^A from the χ^2-minimization and the number N^C of Coulomb-pairs below $|Q_L| < 3$ MeV/c (Table 1) to calculate the breakup probability P_{br} from Eq. (6) with $N^A = k_{exp} \cdot N^C$. The result for $\pi^{\pm}K^{\mp}$ ($P_{br} = 64 \pm 25\%$) is shown by the horizontal solid line in Fig. 8. This leads to a lower limit for the mean life of πK-atoms of $\tau_{1S} = 0.8$ fs at a confidence level of 90%. This result can be translated into an upper limit $|a_{1/2} - a_{3/2}| < 0.58 m_\pi^{-1}$ at 90% confidence level, in agreement with predictions [8,9].

5. Conclusions

We have presented the first evidence for the production of πK-atoms by detecting 173 ± 54 atomic-pairs. The evidence is strengthened by the observation of correlated πK (continuum) Coulomb-pairs from which the number of bound states (atoms) is predicted and found to be in agreement with observation. A lower limit on the mean life of 0.8 fs is established with a confidence level of 90%. We note that the choice of Pt as production target was driven by the high breakup probability facilitating the observation of πK-atoms. Data are now being collected for a more accurate measurement of the lifetime with e.g. a 98 μm Ni-target, for which the breakup probability is lower ($\sim$35% according to Ref. [15]) but still rapidly rising around the predicted mean life of 3.7 fs. The ultimate goal of the experiment is to measure the lifetime of πK-atoms with a precision of about 20% [15].

Acknowledgements

References

[1] S. Weinberg, Phys. Rev. Lett. 17 (1966) 616.
[2] J. Gasser, H. Leutwyler, Nucl. Phys. B 250 (1985) 465;
    J. Gasser, H. Leutwyler, Nucl. Phys. B 250 (1985) 517;
    J. Gasser, H. Leutwyler, Nucl. Phys. B 250 (1985) 539.
[3] G. Colangelo, J. Gasser, H. Leutwyler, Nucl. Phys. B 603 (2001) 125.
[4] L. Afanasyev, et al., Phys. Lett. B 338 (1994) 478.
[5] B. Adeva, et al., Phys. Lett. B 619 (2005) 50.
[6] S. Descotes-Genon, L. Girlanda, J. Stern, JHEP 0001 (2000) 041;
    S. Descotes-Genon, L. Girlanda, J. Stern, Eur. Phys. J. C 27 (2003) 115.
[7] S.M. Bilen'kii, N. van Hieu, L.L. Nemenov, F.G. Tkebuchava, Yad. Fiz. 10 (1969) 812, Sov. J. Nucl. Phys. 10 (1969) 469.
[8] J. Schweizer, Phys. Lett. B 587 (2004) 33.
[9] P. Büttiker, S. Descotes-Genon, B. Moussallam, Eur. Phys. J. C 33 (2004) 409.
[10] P. Estabrooks, et al., Nucl. Phys. B 133 (1978) 490.
[11] V. Bernard, et al., Nucl. Phys. B 357 (1991) 129.
[12] L.L. Nemenov, Yad. Fiz. 41 (1985) 980, Sov. J. Nucl. Phys. 41 (1985) 629.
[13] O.E. Gorchakov, et al., Yad. Fiz. 63 (2000) 1936, Phys. At. Nucl. 63 (2000) 1847.
[14] B. Adeva, et al., Nucl. Instrum. Methods A 515 (2003) 467.
[15] B. Adeva, et al., Addendum to the DIRAC proposal, CERN-SPSC-2004-009, SPSC-P-284 Add.4.
[16] A. Kuptsov, DIRAC note 08-01 http://dirac.web.cern.ch/DIRAC/i_notes.html.
[17] V. Brekhovskikh, et al., DIRAC note 08-02, http://dirac.web.cern.ch/DIRAC/i_notes.html.
[18] S. Horikawa, et al., Nucl. Instrum. Methods A 595 (2008) 212.
[19] Y. Allkofer, et al., Nucl. Instrum. Methods A 582 (2007) 497.
[20] Y. Allkofer, et al., Nucl. Instrum. Methods A 595 (2008) 84.
[21] L. Afanasyev, et al., Nucl. Instrum. Methods A 491 (2002) 376.
[22] D. Drijard, M. Hansroul, V. Yazkov, The DIRAC Offline User Guide, see http://dirac.web.cern.ch/DIRAC/.
[23] Y. Allkofer, PhD Thesis, Universität Zürich, 2008.
[24] Y. Allkofer, A. Benelli, L. Tauscher, DIRAC note 07-09, http://dirac.web.cern.ch/DIRAC/i_notes.html.
[25] Y. Allkofer, A. Benelli, L. Tauscher, DIRAC note 07-08, http://dirac.web.cern.ch/DIRAC/i_notes.html.
[26] B. Adeva, et al., Nucl. Instrum. Methods A 491 (2002) 41.
[27] A.D. Sakharov, Zh. Eksp. Teor. Fiz. 18 (1948) 631.
[28] R. Lednicky, nucl-th/0501065.
[29] L. Afanasyev, O. Voskresenskaya, Phys. Lett. B 453 (1999) 302.
[30] O. Gorchakov, P. Zrelov, V. Yazkov, GEANT-DIRAC simulation, http://dirac.web.cern.ch/DIRAC/.